Journal of Applied Electrochemistry (2022) 52:989–1002
https://doi.org/10.1007/s10800-022-01684-z

RESEARCH ARTICLE

A novel enhanced electrochemical sensor based on the peroxidase-like activity of Fe_3O_4@Au/MOF for the detection of p-aminophenol

Huanan Guan[1] · Yue Zhang[1] · Shuping Liu[1]

Received: 18 November 2021 / Accepted: 6 February 2022 / Published online: 15 February 2022

Abstract

A new type of composite metal–organic framework (Fe_3O_4@Au/MOF) nanoparticle was prepared by self-assembly method, which had the recyclability of Fe_3O_4 magnetic particles (Fe_3O_4NPs) and the advantage of gold nanoparticles (AuNPs) that could accelerate electron transfer. In addition, the mimic enzyme activity of Fe_3O_4@Au/MOF has been significantly increased because of the presence of Fe_3O_4NPs and AuNPs. Then physical and chemical characterization of the composite nanoparticle was carried out through advanced technologies, such as Fourier transform infrared spectroscopy, transmission electron microscope and X-ray photoelectron spectroscopy. Finally, based on the peroxidase-like activity enhanced by Fe_3O_4@Au/MOF composite nanoparticle, a highly specific enzyme-free electrochemical sensor was prepared for the detection of p-aminophenol. The results showed that the optimal catalytic system was the reaction temperature of 50 °C, the addition amount of Fe_3O_4@Au/MOF of 0.005 g, scanning rate of 0.1 V s^{-1}, and buffer solution pH 5. The working curve equation is $|I_{pa}| = 2.7372C + 2.1068$, R^2 was 0.9952, and the minimum detection limit was 0.38 μmol L^{-1} ($S/N = 3$) when the p-aminophenol concentration was located in the range of 0.1–10 mmol L^{-1}. The detection system possessed an excellent recovery rate and anti-interference. In addition, the proposed method was validated to determine p-aminophenol in water samples with satisfactory results.

✉ Huanan Guan
guanhuanan3@163.com

[1] College of Food Engineering, Harbin University of Commerce, Harbin 150028, Heilongjiang, People's Republic of China

Graphical abstract

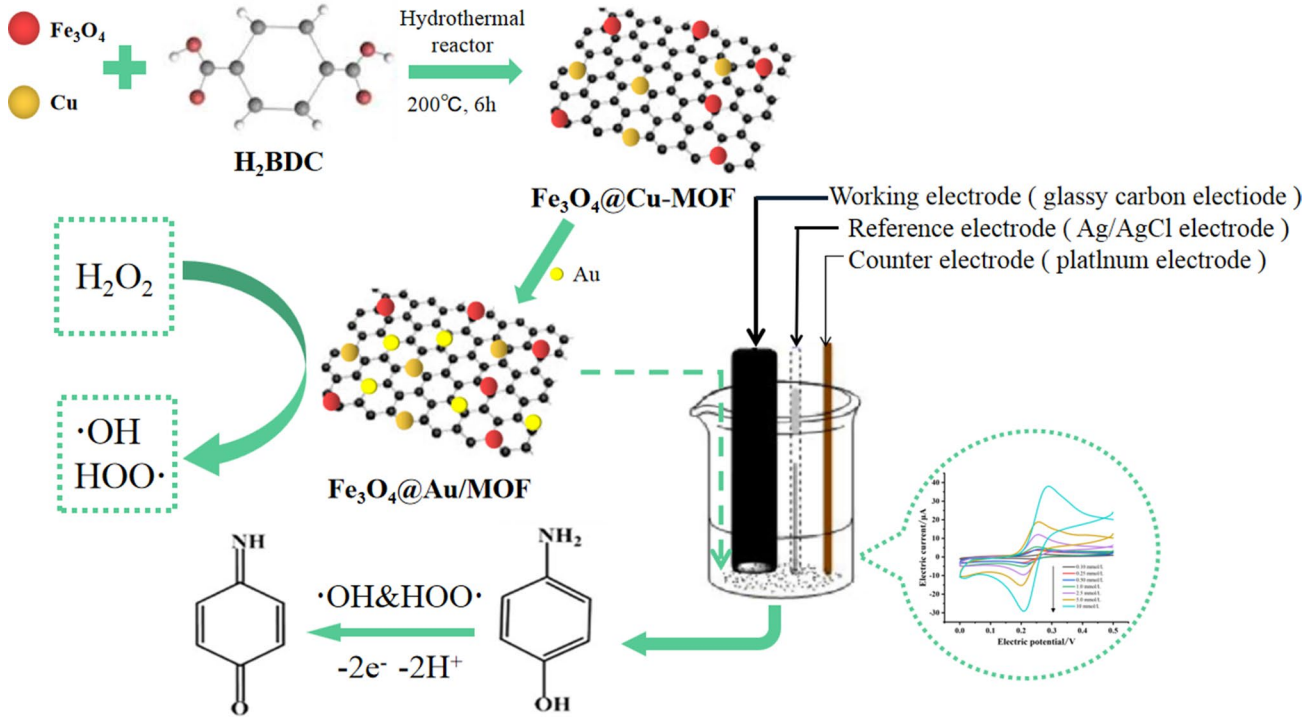

Keywords Metal–organic framework · Mimic enzyme · Electrochemical sensor · P-aminophenol

1 Introduction

P-aminophenol, also named 4-aminophenol (4-AP), belongs to the phenolic compound, a widely used industrial raw material and an important intermediate of fine chemicals [1]. Meanwhile, p-aminophenol is a significant impurity present in the paracetamol containing pharmaceuticals [2, 3]. Thus, the decomposition of paracetamol could lead to the formation of p-aminophenol. In addition, p-aminophenol always is widely used in various fields, such as petroleum, rubber, photography, feeding stuff, sulfur, and azo dyes [4, 5]. Thus, there is a high possibility to contaminate the environment, especially the water bodies with p-aminophenol [6, 7]. What's more, p-aminophenol is harmful to humans due to its nephrotoxic, teratogenic, and mutagenic effects and DNA cleavage in living organisms [8]. Thus, it is a necessity to establish a fast, sensitive, simple, and economical analytical method for detecting p-aminophenol in the water bodies, which is of great significance for environmental protection and human health. At present, the detection methods of p-aminophenol mainly include chromatography [9], spectrophotometry [10, 11], capillary electrophoresis [12, 13], fluorescence analysis [14], and colorimetry [15, 16]. However, all these instrumentation techniques are expensive, time-consuming laboratory processes, difficult detection procedures and need well-equipped skilled persons. Compared to the above method, the electrochemical analysis has the advantages of simple detection, high sensitivity, low detection cost, and real-time monitoring [17, 18]. Therefore, it is a good method for the detection of p-aminophenol.

Compared with the natural enzymes that are prone to inactivation, artificially synthesized materials with enzyme-like activity instead of natural enzymes have attracted widespread attention [19]. Among them, metal–organic frames (MOFs) are considered to be ideal materials for simulating enzymes [20]. The metal–organic framework is a nanohybrid material with a porous network structure formed by the self-assembly of metal ions or metal clusters and organic ligands through coordination bonds [21]. The metal clusters or metal ions in MOFs are generally transitioning metal ions and lanthanide ions, while organic ligands usually contain functional groups, such as pyridine and cyano groups, crown ethers, polyamines, phosphonates, and carboxylates. These functional groups act as a bridge connecting metal ions in MOFs [22].

In recent years, the research of metal–organic framework as mimic enzymes has received more and more

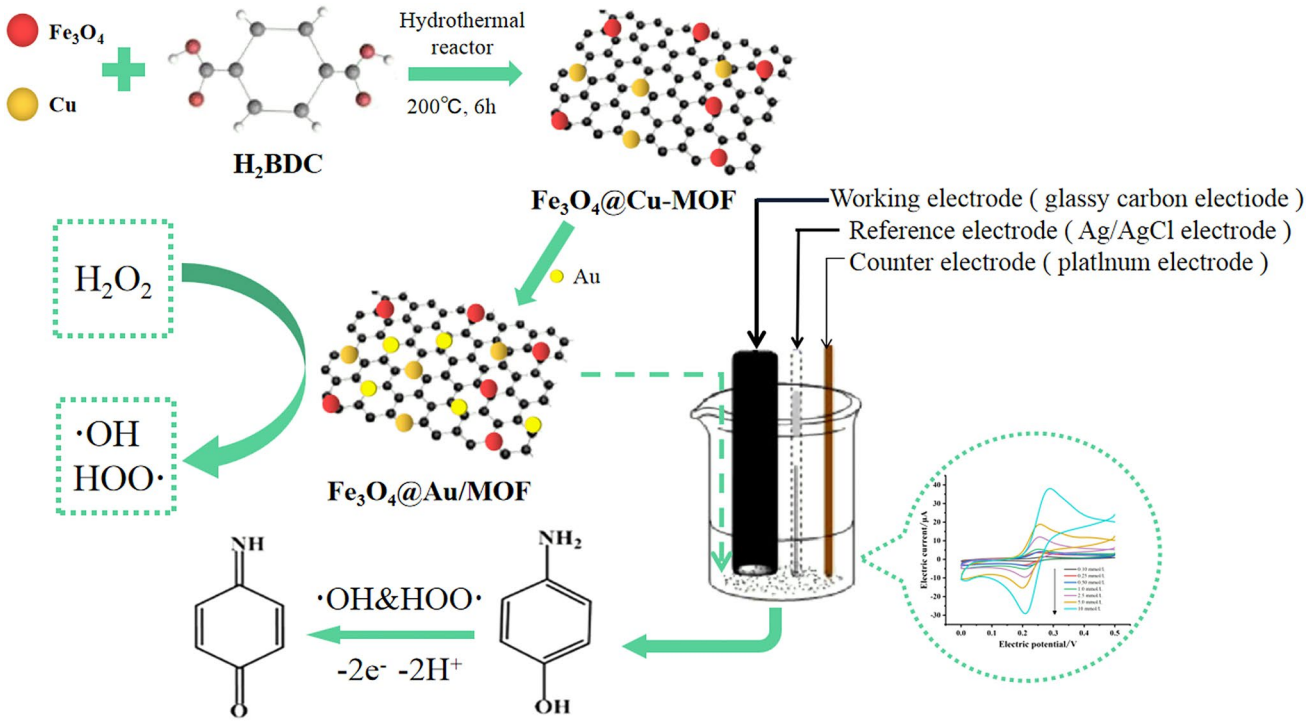

Fig. 1 Schematic illustration of the enhanced electrochemical detection of p-Aminophenol based on the Fe_3O_4@Au/MOF

attention. Compared with natural enzymes, MOFs have obvious advantages, such as low cost, stable structure, easy storage, and adjustable activity [23]. However, compared with other composite MOFs, single MOFs exhibit poorer enzymatic activity. Therefore, other nanomaterials are usually added on the basis of single MOFs to prepare composite MOFs to improve enzymatic activity [24]. Among many nanomaterials, Fe_3O_4 magnetic particles and gold nanoparticles have peroxidase-like activity [25, 26]. Adding to the MOFs could significantly increase the peroxidase-like activity of composite nanoparticles. In addition, Fe_3O_4, as a biocompatible magnetic material, can be recycled and reused by magnets [27, 28]. Gold nanoparticles can amplify and accelerate electron transfer through tuning signals, greatly enhancing the sensitivity and selectivity of electrochemical sensors [29, 30]. Therefore, composing of Fe_3O_4 magnetic particles and gold nanoparticles combined and single MOFs, nanoparticle composite materials have all the advantages of these materials, which they can be more widely used. The previous research results of our team showed that Fe_3O_4 magnetic particles and gold nanoparticles have good peroxidase-like activity and catalytic performance, so they are chosen to be added to the metal–organic framework [31–33].

In this paper, the copper-based metal–organic framework (Fe_3O_4@Cu-MOF) was synthesized by dispersing Fe_3O_4 magnetic particles and transition metal copper ions (Cu^{2+}) in a two-dimensional network structure formed by terephthalic acid (PTA). The metal–organic framework mimic enzyme (Fe_3O_4@Au/MOF) with enzymatic-like activity was prepared after gold nanoparticles (AuNPs) were embedded in the network structure. There are previous studies reported to illustrate that H_2O_2 can be catalyzed due to the mechanism of Cu-MOF with exposed active sites. However, compared to monometallic–organic frameworks, composite metal–organic frameworks incorporating multimetal elements have better enzyme-like activities. Therefore Fe_3O_4 magnetic particles and AuNPs were added on the basis of Cu-MOF to make Fe_3O_4@Au/MOF possess multiply enhanced peroxidase-like activity. In addition, due to the network structure of Cu-MOF, it can be effective as a support to prevent the activity decrease resulting from metal particle aggregation. In Fe_3O_4@Au/MOF, Fe_3O_4 magnetic particles not only function in enhancing enzyme-like activity but also allow Fe_3O_4@Au/MOF to be recycled for reuse due to its magnetism. Similarly, in the Fe_3O_4@Au/MOF, AuNPs not only play the role of peroxidase-like enzymes but can also tune the signal to make the sensor sensitive to capture the transfer of electrons from the system. As shown in Fig. 1, it described the working principle of the electrochemical method for p-aminophenol detection based on Fe_3O_4@Au/MOF peroxidase-like mimetic catalytic activity. Fe_3O_4@Au/MOF catalyzed the decomposing H_2O_2 to release hydroxyl radicals with oxidative activity, which further accelerated

the oxidation reaction of electrochemical signal substance p-aminophenol on the surface of the glassy carbon electrode, thereby increasing the movement of charges in the system. Based on this principle, a Fe_3O_4@Au/MOF mimic enzyme-enhanced electrochemical p-aminophenol detection system was constructed. Finally, it was successfully used for the detection of p-aminophenol in water samples. In addition, electrochemical sensors based on Fe_3O_4@Au/MOF possessed the advantages of sensitivity, high efficiency, good selectivity, and high stability. Due to the recyclability of Fe_3O_4@Au/MOF, the sensor also exposed the advantage of low cost. Therefore, the current work provided an effective p-aminophenol measurement method, which could broaden the application prospects in the fields of environmental analysis and biomedicine.

2 Experimental

2.1 Reagents and instruments

P-aminophenol was obtained from Guangfu Fine Chemical Research Institute. (Tianjin, China). Ferric chloride hexahydrate ($FeCl_3{\cdot}6H_2O$), ethylene glycol ($C_2H_6O_2$), acetic acid sodium salt trihydrate ($NaAc{\cdot}3H_2O$), Chloroauric acid ($HAuCl_4$), and Copper sulfate ($CuSO_4$) were all purchased from Kemiou Chemical Reagent Co., Ltd. (Tianjin, China). Polyvinylpyrrolidone (PVP) and polyethylene glycol (PEG-4000) were all sourced from Gongbike New Material Technology Co., Ltd. (Shanghai, China). N,N-dimethylformamide (DMF) was purchased from Yubo Biochemical Co., Ltd. (Luohe, China). Terephthalic acid (H_2BDC) was obtained from Oen Ruisi Chemical Reagent Co., Ltd. (Chengdu, China). Sodium borohydride ($NaBH_4$) was sourced from Hongrui Chemical Co., Ltd. (Shanghai, China). 2,2'-azino-bis(3-ethylbenzothiazoline-6-sulfonic acid) (ABTS) was obtained from Shanghai Aladdin Bio-Chem Technology Co., Ltd (Shanghai, China). All the chemicals used were of analytical grade and used as received. Acetic acid and sodium acetate were used to configure the buffer solution that was required in the reaction. The buffer solution with a total concentration of 1 mol L^{-1} was prepared according to the ionization equation of acetic acid and sodium acetate and the calculation formula of pH. The pH value was changed by adjusting the volume of acetic acid and the mass of sodium acetate.

P-aminophenol is detected by a CHI660E electrochemical workstation (Shanghai Chenhua Instrument Co., Ltd., China), which is equipped with a three-electrode cell was used for the electrochemical characterization and sensing applications, including a bare glass carbon electrode (GCE) with a diameter of 5 mm as the working electrode, a platinum electrode as the counter electrode, and the silver electrode (Ag/AgCl) as a reference electrode. During the experiment, the buffer solution added to the electrochemical cell was 10 mL.

The metal–organic framework was synthesized in an YH-1019 hydrothermal reactor (Henan Yuhua Instrument Technology Co., Ltd., China). The appearance characteristics and particle size of the nanoparticles were exposed on the F200X S transmission electron microscope (TEM) image (Oubotong Optical Technology Co., Ltd., Beijing). The bonds between the molecules were recorded on the EDK 9500 Fourier Transform Infrared (FT-IR) spectrometer (Duke Tech, Beijing) and X-ray photoelectron spectroscopy (XPS).

2.2 Synthesis of Fe_3O_4@Au/MOF

Firstly, the preparation of Fe_3O_4 nanoparticles by hydrothermal method referred to a document with minor modification [32]. Adding 3 g $FeCl_3{\cdot}6H_2O$, 6.3 g $NaAc{\cdot}3H_2O$, and 1.8 g PEG-4000 to a beaker containing 80 mL ethylene glycol. Pouring the homogeneous mixed solution into a hydrothermal reaction kettle after thoroughly shaking for 30 min and keeping it at 200 °C for 8 h. After cooling at room temperature, washed with ethanol and deionized water until pure and dried to constant weight.

Fresh orange peel was used as the material to prepare gold nanoparticles using a modified green reduction method [33], soaked 20 g of chopped orange peels in deionized water at 80 °C for 1 h and then centrifuged the filtrate at 3500 r min^{-1} for 5 min to obtain the supernatant. Diluted the supernatant with deionized water to obtain an orange peel backup solution and stored it at 4 °C. 20 mL of pre-cooled 4 °C chloroauric acid was placed in a beaker by stirring evenly using a magnetic stirrer and quickly added 5 mL of orange peel backup solution into the beaker. With the continuous increase of the stirring speed, the color of the system changed from yellow to wine red. The reactions were completed when the color does not change within 30 min. It is worth noting that the synthesized nanogold solution needs to be stored at 4 °C.

At last, 2 g of synthesized Fe_3O_4 nanoparticles and 10 mL of standard ethanol solution were thoroughly mixed in a shaker for 30 min. Then add 3 g of polyvinylpyrrolidone (PVP), 20 mL of standard ethanol solution, and 45 mL of N,N-dimethylformamide (DMF) in it and perform ultrasonic treatment for 45 min. After that, 10 mL of the bivalent copper ion standard solution and 2 g of terephthalic acid powder were added and fully reacted with shaking in a shaker for 30 min. The mixed solution was placed in a high-temperature hydrothermal reactor at 200 °C for 6 h. The standard ethanol solution and distilled water were used for multiple pieces of washing of the mixed solution until the washing

water became clear. Finally, the cleaned metal–organic frame (Fe_3O_4@Cu-MOF) was placed in a drying box and dried to a constant weight. After Fe_3O_4@Cu-MOF was ultrasonically dispersed in 5 mL of distilled water, 5 mL of gold nanoparticle solution was added to it, and placed in a shaker for 6 h. Then 10 mL of sodium borohydride aqueous solution with a concentration of 0.1 mol L^{-1} was added and sonicated for 45 min. Finally, distilled water was used to wash it and Fe_3O_4@Au/MOF two-dimensional magnetic metal–organic framework was obtained after drying to constant weight.

2.3 Verification of Fe_3O_4@Au/MOF mimic enzyme activity

Five different reaction systems were prepared to verify the mimics enzyme activity of Fe_3O_4@Au/MOF in the electrochemical system: (a) buffer solution + H_2O_2 + Fe_3O_4@Au/MOF; (b) buffer solution + 4-AP; (c) buffer solution + 4-AP + Fe_3O_4@Au/MOF; (d) buffer solution + H_2O_2 + 4-AP; and (f) buffer solution + H_2O_2 + 4-AP + Fe_3O_4@Au/MOF. The CV method was used to monitor the change of (a) → (f) oxidation peak current.

Then, the kinetics of the catalytic reaction of Fe_3O_4@Au/MOF was further studied by colorimetric method. Changed the concentration of substrate H_2O_2 (0–50 mmol L^{-1}) and ABTS (0.1–2.0 mmol L^{-1}) to collect absorbance data. The maximum absorption wavelength of ABTS is 420 nm. The enzyme-like kinetics of Fe_3O_4@Au/MOF was evaluated by the steady-state kinetics method and constructed double the reciprocal curve to calculate the reaction kinetic parameters. According to the obtained data, the Lineweaver–Burk diagram is made and calculated the Michaelis constant by the formula of $1/V_0 = K_m/V_{max}$ $(1/[S] + 1/K_m)$.

2.4 Electrochemical detection of p-aminophenol

P-aminophenol detection was done as follows: (a) 0.1 g of Fe_3O_4@Au/MOF powder and 600 μL of H_2O_2 (50 mmol L^{-1}) in HAC-NaAC buffer solution (pH = 5) were reacted at 50 °C for 5 min. (b) The reaction was initiated by the addition of 400μL of p-aminophenol (1 mmol L^{-1}). (c) The oxidation–reduction reaction of p-aminophenol sensing on the surface of the GCE was performed by recording the cyclic voltammograms at a scan rate of 0.1 V s^{-1} in the potential range of 0–0.5 V.

Investigated the influence of four factors on the detection system of p-aminophenol to obtain the best detection system, including temperature (20, 30, 40, 50 and 60 °C), pH value (4, 5, 6, 7 and 8), scan rate (0.02, 0.04, 0.06, 0.08 and 0.1 V s^{-1}) and Fe_3O_4@Au/MOF addition amount (0.0025, 0.0050, 0.0075, 0.01 and 0.0125 g). Under optimized conditions, researched the electrochemical behavior of p-aminophenol on the surface of the glassy carbon electrode from the concentration of 0.1–10 mmol L^{-1} and established the work curve of p-aminophenol with the concentrations as the abscissa and $|I_{pa}|$ as the ordinate. Furthermore, based on the p-aminophenol working curve, the LOD and recovery rate of the detection system were calculated. Then under the best detection system, the interference of several common substances in the water on the electrochemical detection system was investigated.

2.5 Real sample analysis

The p-aminophenol was quantified in laboratory tap water samples by addition and recovery experiments. Detected the $|I_{pa}|$ of tap water samples with three different concentrations of p-aminophenol standard solutions respectively. The results of the detection of p-aminophenol by electrochemical method and high-performance liquid chromatography (HPLC) were compared and then repeated the experiment to determine the recovery rate of standard addition and evaluate the detection system's accuracy.

3 Results and discussion

3.1 Characterization of Fe_3O_4@Au/MOF

The morphology of Fe_3O_4@Au/MOF was observed by TEM (Fig. 2). Figure 2 shows the TEM images of Fe_3O_4@Au/MOF metal–organic framework at different resolutions. The images revealed that the average particle size of the nanoparticles was 8–15 nm and the diameter of the large clusters composed of scattered spheres with rough surfaces was about 600 nm. According to the comparison of Fig. 2b and c, it is found that the magnetic particles and gold nanoparticles are dispersed in the clusters without aggregation, indicating that the copper-based metal–organic framework can effectively isolate the aggregation between large metal particles. Meanwhile, magnetic particles and gold nanoparticles were successfully combined with copper-based metal–organic frameworks, which enhanced the catalytic activity of the composite nanoparticles.

XPS was used further to analyze the composition of Fe_3O_4@Au/MOF. In the XPS spectrum, the three prominent peaks were Fe 2p, Au 4f, and Cu 2p, respectively. The high-resolution XPS spectrum of Fe 2p contained two binding energies, 710.55 and 724.32 eV, respectively (Fig. 3). These two binding energies represented the bimodal Fe $2P_{3/2}$ and Fe $2P_{1/2}$, which were characteristic of Fe_3O_4 magnetic particles (Fig. 3a). The spectrum of Au 4f region can be observed at 93.55 eV, which indicates that AuNPs maintain a metallic state in the system solution (Fig. 3b) [34]. The spectrum of

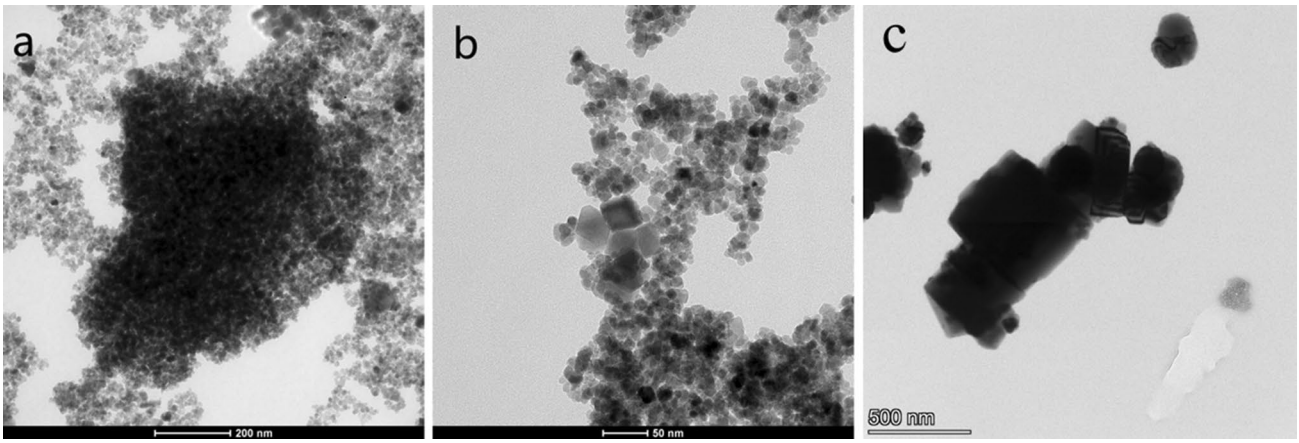

Fig. 2 Transmission electron microscopy (TEM) images of Fe_3O_4@Au/MOF with the scale bar 200 nm (**a**), 50 nm (**b**) and Fe_3O_4 with the scale bar 500 nm (**c**)

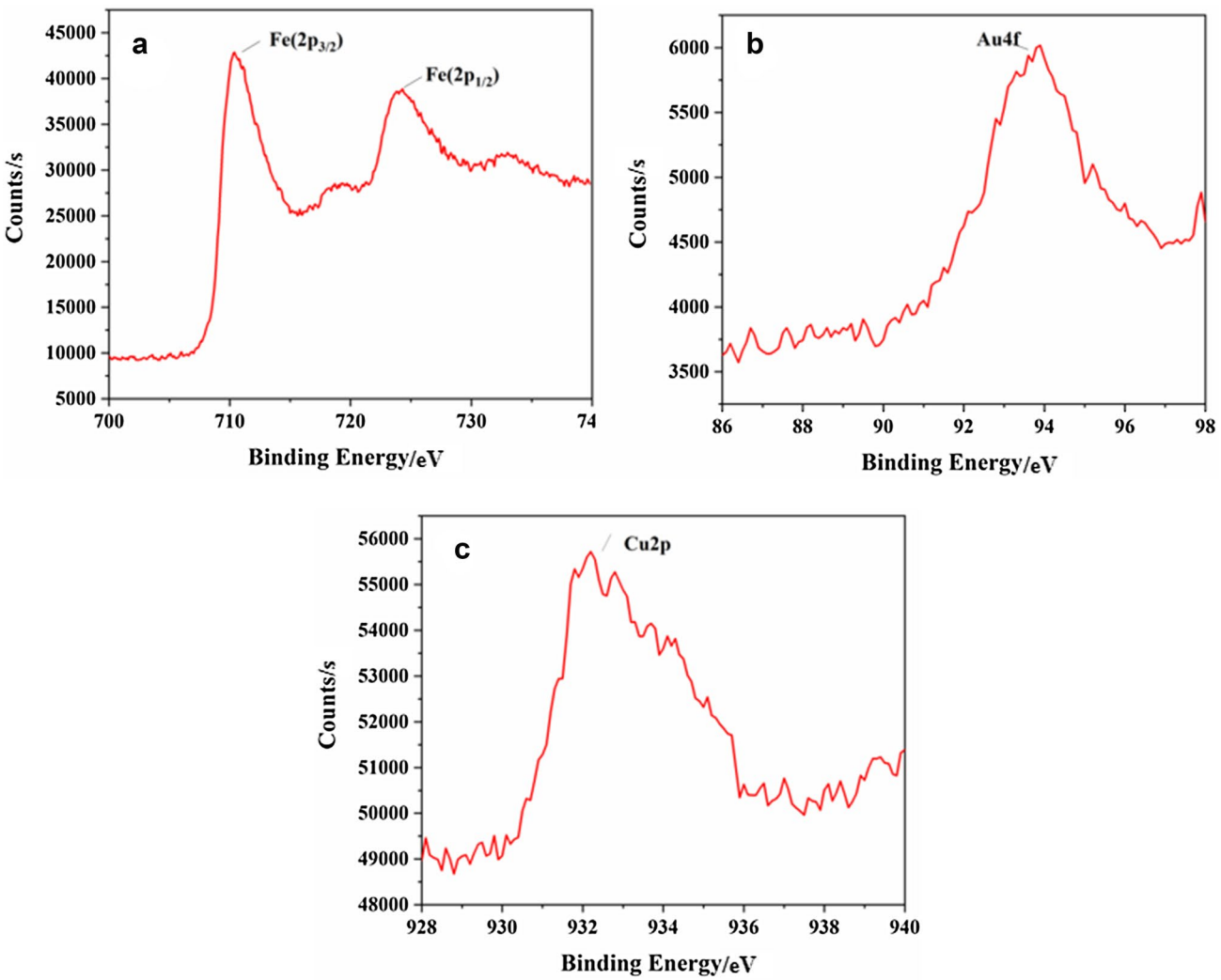

Fig. 3 XPS spectra in the regions of Fe2p (**a**), Au4f (**b**), and Cu2p (**c**) for Fe_3O_4@Au/MOF

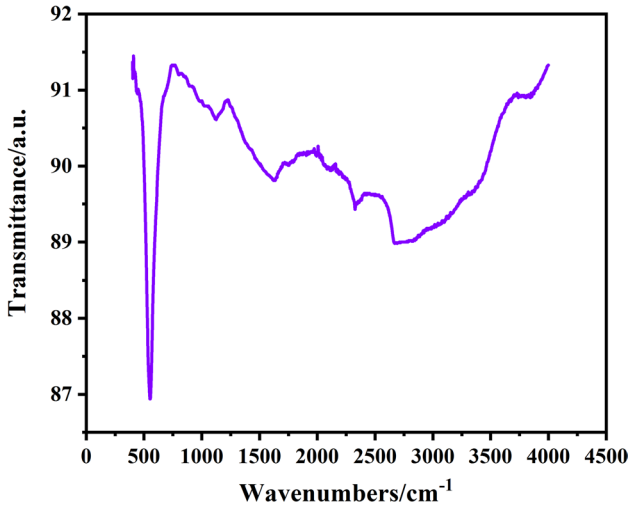

Fig. 4 Fourier infrared spectrum of Fe_3O_4@Au/MOF

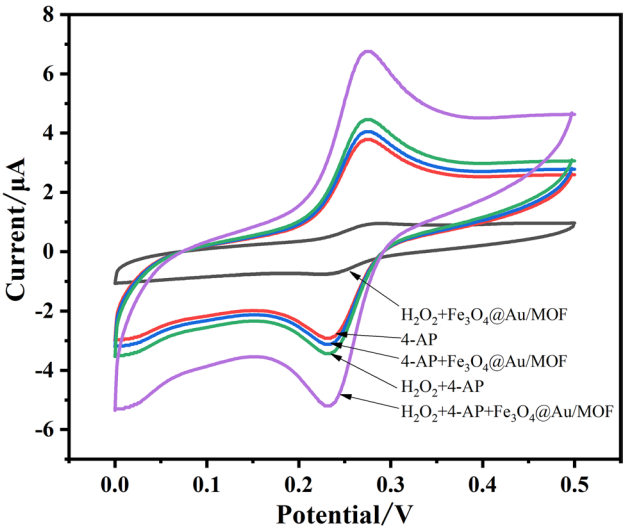

Fig. 5 CV curve of Fe_3O_4@Au/MOF peroxidase activity

Cu 2p region can be observed at 932.52 eV, which is consistent with the standard binding energy of metal Cu (Fig. 3c) [35]. It means that the synthesized composite nanomaterials successfully contain Fe_3O_4NPs, AuNPs, and Cu^{2+}.

We carried out FT-IR measurements on the Fe_3O_4@Au/MOF [32], as shown in Fig. 4. For Fe_3O_4@Au/MOF, the peak at 560.19 cm^{-1} could be attributed to the vibration of the Fe–O bond in magnetic particles. The absorption peak of about 1117.31 cm^{-1} was put down to the C–O stretching. In addition, the absorption peak at 1631.33 cm^{-1} could be due to the presence of amino groups. The two absorption peaks between the wavelengths of 2250–2750 cm^{-1} could be by the vibration of the long-chain alkyl groups $–CH_2$ and $–CH_3$. Moreover, the peak at 3846.44 cm^{-1} could be attributed to the characteristic peak of –OH bond with specific catalytic oxidation.

3.2 Analysis of simulated enzyme activity of Fe_3O_4@Au/MOF composite particles

To investigate the peroxidase-like activity of Fe_3O_4@Au/MOF, Fe_3O_4@Au/MOF was evaluated by the catalytic redox reactions of p-aminophenol in the presence of H_2O_2. As shown in Fig. 5, the low-concentration H_2O_2 cannot produce the oxidation current peak in the presence of Fe_3O_4@Au/MOF, indicating that there was no movement of electrons on the surface of the glassy carbon electrode or the reaction in the system was not enough to generate the current response. When only p-aminophenol was present in the HAc-NaAc buffer system, a weak electrochemical signal was generated, attributed to the unique electrochemical activity of p-aminophenol [36]. Both the 4-AP + Fe_3O_4@Au/MOF buffer solution system and the H_2O_2 + 4-AP buffer solution system produced prominent oxidation peak currents and the current response showed an increasing trend. The results showed that H_2O_2 and Fe_3O_4@Au/MOF could, respectively, catalyze the redox reaction of p-aminophenol to different degrees. It is worth noting that Fe_3O_4@Au/MOF catalyzed several oxidizing substances in the solution and reacted with p-aminophenol, promoting electron transfer. Thus reflected the activity of peroxidase mimics. The Fe_3O_4@Au/MOF + H_2O_2 + 4-AP system had a significantly amplified peak oxidation current compared to other systems. It indicated that Fe_3O_4@Au/MOF, as a peroxidase mimetic enzyme, catalyzed H_2O_2 to reintroduce a large amount of oxidative active substances (mainly ·OH and HOO· free radicals with oxidative activity), which significantly further promoted the oxidation of p-aminophenol. In addition, since Fe_3O_4@Au/MOF contains a small amount of Fe_3O_4NPs, the Fenton reaction also occurs in the system in the presence of H_2O_2. When Fe_3O4@Au/MOF catalyzes H_2O_2 to produce a large amount of ·OH, its Fe^{3+} will be converted into Fe^{2+} and the generated Fe^{2+} can trigger Fenton reaction with the ·OH generated in the catalytic process. After the Fenton reaction is completed, Fe^{2+} will be converted into Fe^{3+} to become cyclic catalysis. During this process, due to the synergistic effect of Fe_3O_4@Au/MOF catalytic reaction and Fenton reaction of Fe_3O_4NPs, a large number of active hydroxyl radicals exist in the system. The redox reaction involves a reversible transfer process of two protons and two electrons, so that the p-aminophenol would be oxidized to 1,4-benzoquinone [8]. The results demonstrated that under normal circumstances, p-aminophenol might undergo a small degree of oxidation. However, Fe_3O_4@Au/MOF composite particles could catalyze hydrogen peroxide to produce free radicals with oxidative activity in the presence of hydrogen peroxide, which could significantly

promote the redox reaction of p-aminophenol. In summary, it can be proved that Fe_3O_4@Au/MOF exhibited peroxidase-like activity, which can effectively catalyze H_2O_2 and further oxidize p-aminophenol. Therefore, it can be added to the electrochemical detection of p-aminophenol to speed up.

3.3 Catalytic kinetic analysis of Fe_3O_4@Au/MOF enzyme-like activity

The evaluation results of enzyme-like kinetics of Fe_3O_4@Au/MOF composite nanomaterials are shown in Fig. 6. As shown in Fig. 6a and b, within a certain concentrations range of H_2O_2 or ABTS, the initial velocity of the catalytic reaction gradually increases as the substrate concentrations increase. Moreover, it tended to be constant under high concentrations of substrate. The enzymes were almost saturated with the substrates, which follows the typical Michaelis–Menten mechanism. Then made the Lineweaver–Burk double reciprocal diagrams (Fig. 6c, d) to calculate the constant (K_m) and the maximum initial velocity (V_{max}). There is no doubt that K_m is considered to be an essential parameter for evaluating the affinity between the substrates and the enzymes. The smaller the K_m, the stronger the affinity between the enzymes and the corresponding substrates. The calculation results are summarized in Table 1. It is worth noting that compared with horseradish peroxidase (HRP) and other reported nanozymes, Fe_3O_4@Au/MOF had a relatively higher affinity for these two substrates. This could be due to the fact that Fe_3O_4@Au/MOF has multiple catalytically active sites and effective electron transfer pathways on the surface, which greatly improve the catalytic performance of Fe_3O_4@Au/MOF composite particles for H_2O_2 as well as the electrode's capture ability for electron transfer.

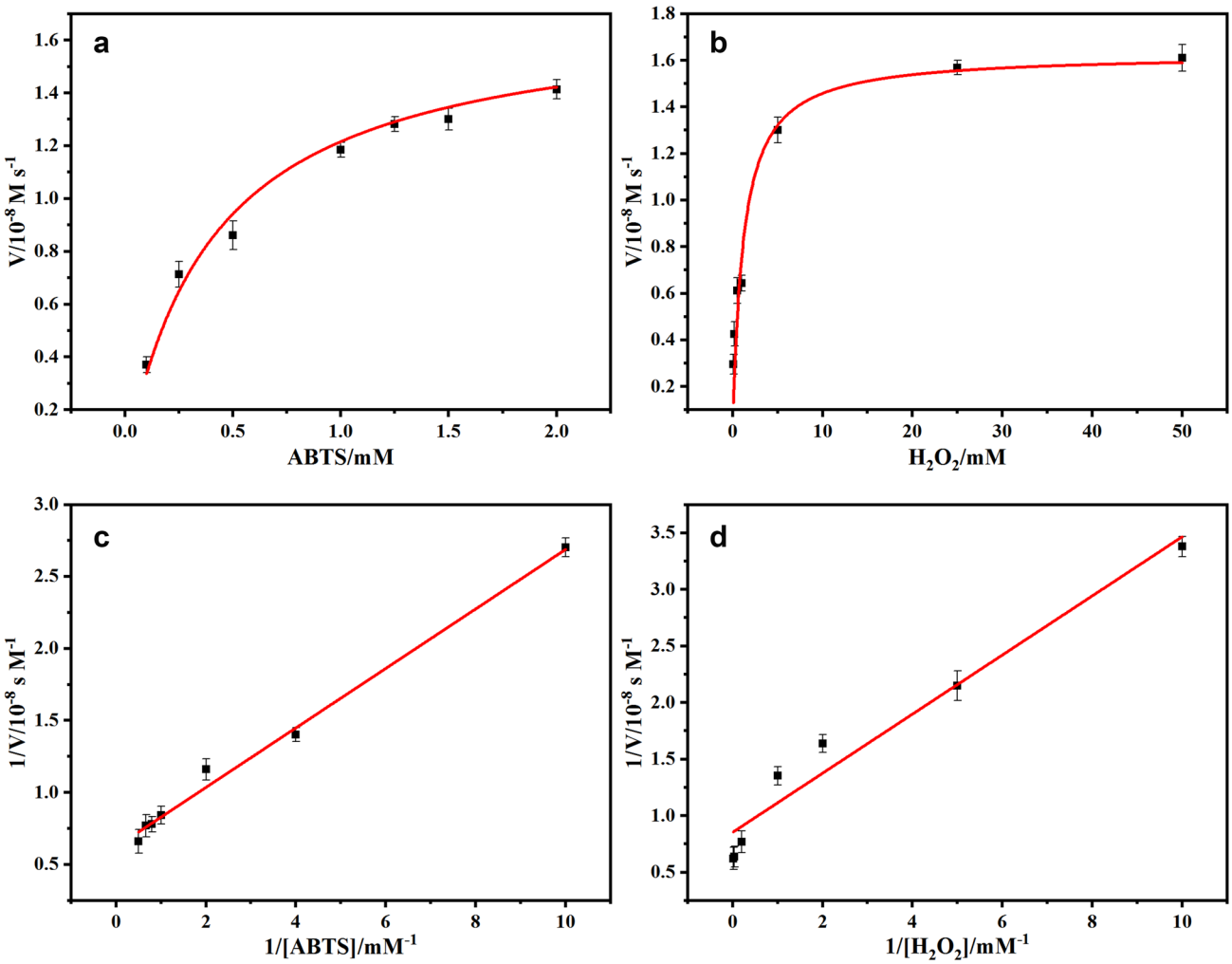

Fig. 6 Steady-state kinetic assay of Fe_3O_4@Au/MOF. Michaelis–Menten curves of Fe_3O_4@Au/MOF on ABTS (**a**) and H_2O_2 (**b**); Lineweaver–Burk linear fit chart of Fe_3O_4@Au/MOF on ABTS (**c**) and H_2O_2 (**d**)

Table 1 Comparison of catalytic kinetic constants

Catalyst	Substrate	K_m/mmol L^{-1}	V_{max}/M s^{-1}	Reference
HRP	H_2O_2	3.7	8.7×10^{-8}	[40]
HRP	ABTS	0.4	1.0×10^{-7}	[40]
$NiFe_2O_4$	ABTS	0.46	17.48×10^{-8}	[41]
MoS_2@ $MgFe_2O_4$	ABTS	1.03	1.41×10^{-8}	[42]
$Co(OH)_2$/ $FeOOH/WO_3$	H_2O_2	6.9	1.97×10^{-7}	[43]
Fe_3O_4@Au/ MOF	H_2O_2	0.131	2.8×10^{-8}	This work
Fe_3O_4@Au/ MOF	ABTS	0.327	1.6×10^{-8}	This work

3.4 Optimization of electrochemical detection conditions

It is well known that the scan rate has an important influence on the sensitivity of electrochemical sensors. This work investigated the impact of different scan rates on detection and the screened appropriate level. The results showed that the $|I_{pa}|$ of p-aminophenol keeps increasing as the scanning rate increases in Fig. 7a. Under the premise of the same scan cycles, the diffusion time of the fixed concentration of p-aminophenol on GCE will change substantially due to the difference of the scan rate. However, the oxidation reaction of p-aminophenol occurs instantaneously, so slightest nuance of time changes can also affect the electron transfer rate during the reaction and the adsorption accumulation process on the surface of GCE. It further proved that the electrochemical processes of p-aminophenol on GCE were diffusion control processes [37]. However, it can be clearly seen that the rate of increase from 0.08 to 0.1 V s^{-1} has been significantly reduced. Although because I_{pa} obeys the Randles–Sevcik equation and will be proportional to square root of scan rate, it means I_{pa} still increases when scan rate increases. However, for the scan rate of the electrochemical

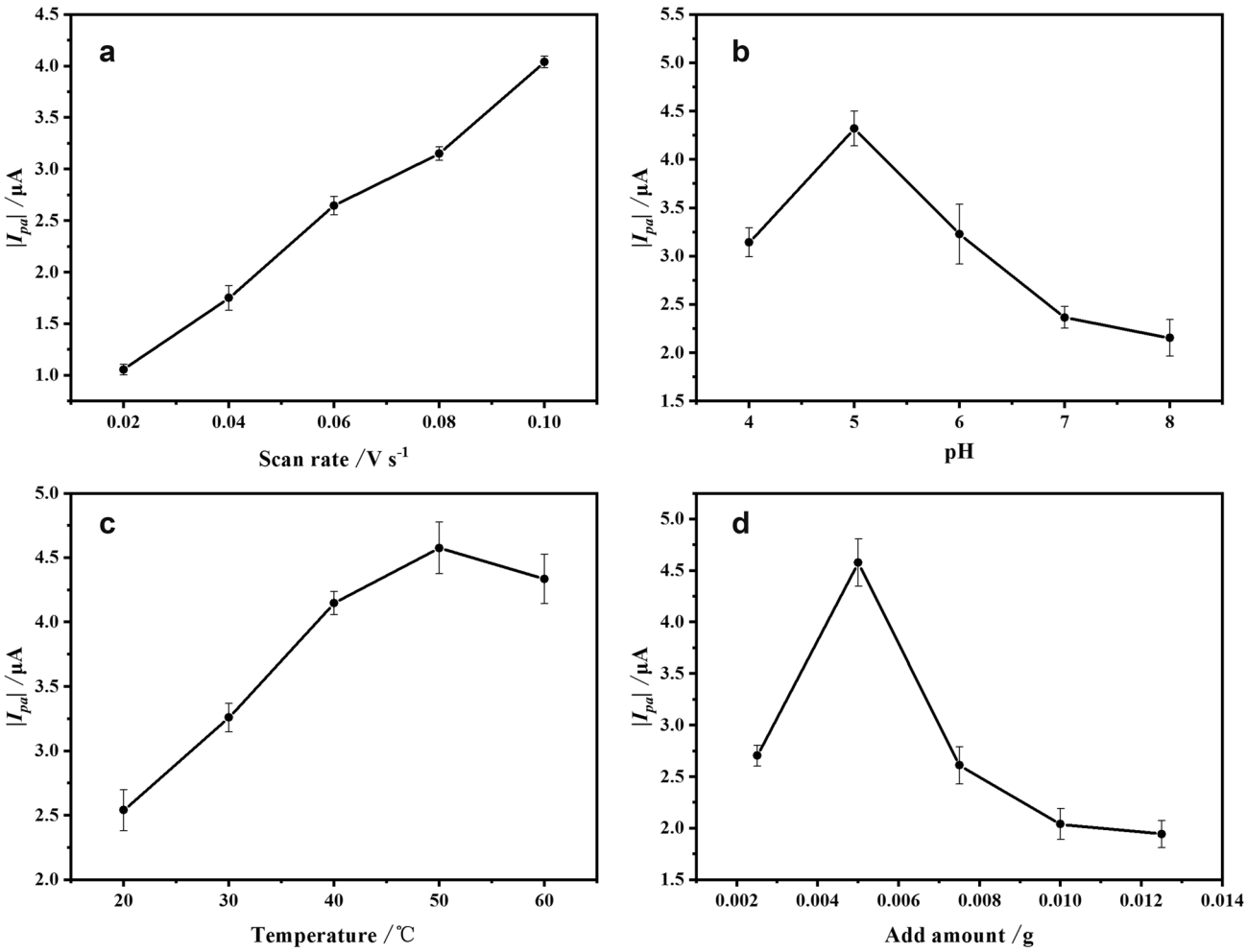

Fig. 7 Effect of scan rate (**a**), pH (**b**), temperature (**c**), and Fe_3O_4@Au/MOF addition (**d**) on the Fe_3O_4@Au/MOF-H_2O_2 system for p-aminophenol detection. The highest point was defined as 100% relative activity

workstation, the previous experimental studies by our team showed that when the scan rate exceeds 0.1 V s^{-1}, the stability of the detection system will be affected, so it means that 0.1 V s^{-1} could be selected as the optimal scan rate rate.

Secondly, since the pH value can directly affect the concentration of protons in the system solution, the influence of pH value on the electrochemically enhanced detection system was investigated. It can be seen from Fig. 7b that the peak oxidation current reached its highest point at pH = 5 and at the same time, the catalytic activity of the Fe_3O_4@Au/MOF was the most significant. As the pH continued to increase, the oxidation peak current showed a significant downward trend when the pH changed in the range of 5–8. This might be due to the fact that the protons in the system continue to decrease with the increase of pH and the protons participate in the redox reaction in the system [38]. Therefore, the amount of electron transfer and the electrochemical response in the system were reduced. This current response behavior suggests that the acidic and basic systems reduce the activity of the electrode, leading to an inhibition of the response. Thus, it is most appropriate to choose pH 5.0 to participate in the following experiment.

In order to investigate the influence of temperature on the detection of p-aminophenol in the system, experiments were designed at five different temperatures. It can be seen from Fig. 7c that the reaction rate increased with the temperature increasing when the temperature was in the range of 20–50 °C. The increase in the number of electrons transferred on the electrode surface contribute to the enhancement of the electrochemical signal, so that $|I_{pa}|$ continued to rise. This might also be that the increase in the solubility of p-aminophenol due to temperature changed, which can fully react with the free radicals generated by Fe_3O_4@Au/MOF catalyzed. When the temperature exceeded 50 °C, the $|I_{pa}|$ decreased, which might be due to the inhibition of Fe_3O_4@Au/MOF mimic enzyme activity at higher temperatures. Therefore, the optimal temperature was 50 °C.

Furthermore, as shown in Fig. 7d, the $|I_{pa}|$ of the system rose suddenly when the addition of Fe_3O_4@Au/MOF was from 0.0025 to 0.0050 g. This means that the amount of Fe_3O_4@Au/MOF greatly affected the reaction rate in the electrochemical-enhanced detection system. At this time, the mimic enzyme activity in the system was enhanced, thereby promoting H_2O_2 to generate more oxidative active free radicals, further accelerating the electron transfer rate and increasing the amount of electron transfer. However, the $|I_{pa}|$ of the system decreased when the addition of Fe_3O_4@Au/MOF continues to increase. When there was a lot of Fe_3O_4@Au/MOF in the system, the nanoparticles will agglomerate further leading to the gradual decrease of the catalytic activity of the composite nanomimetic enzyme.

3.5 Electrochemical system for detection of p-aminophenol

According to the optimal detection conditions obtained above, the behaviors of the redox reaction in the detection system under different concentrations of p-aminophenol were investigated. Figure 8a depicts the incremental relationship between $|I_{pa}|$ and the concentrations of p-aminophenol and made a working curve image to show their linear relationship (Fig. 8b). As observed, $|I_{pa}|$ had an inevitable increasing trend as the concentrations of p-aminophenol analyte increased from 0.1 to 10 mmol L^{-1}. The positive shift of the redox peaks could be attributed to the kinetics of the electrochemical reactions controlled by the adsorption of

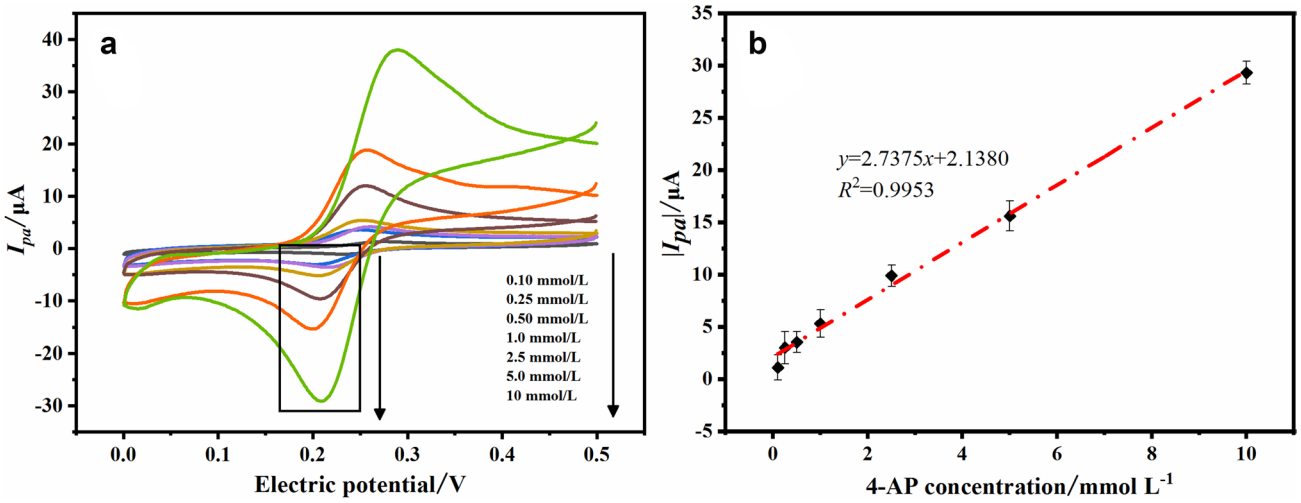

Fig. 8 A response curve for p-aminophenol detection using Fe_3O_4@Au/MOF-H_2O_2 system (**a**). The linear relationship between $|I_{pa}|$ with the p-aminophenol concentrations in the range from 0.1 to 10 mmol L^{-1} (**b**). Error bars represent the standard derivation (SD) of replicates measurements with $n = 3$

p-aminophenol. Moreover, it can be seen from Fig. 8b that p-aminophenol had a good linear relationship with $|I_{pa}|$ in the concentration range of 0.1–10 mmol L^{-1}. The regression equation of the working curve is $|I_{pa}| = 2.7372C + 2.1068$, which had an excellent linear fit and excellent dependence ($R^2 = 0.9952$), as well as the detection limit of 0.38 μmol L^{-1} ($S/N = 3$). In order to evaluate the analytical practicability of the electrochemical detection system, under the optimized electrochemical-enhanced detection system, the recovery rate of the aminophenol standard solution (0.25, 0.5, and 1 mmol L^{-1}) was evaluated according to the obtained working curve regression equation. The recovery rate was calculated to range from 98.6 to 105.3%. And the RSD was less than 2.38%, which indicated the degree of mutual consistency of the results of several parallel determinations. It meant that the electrochemical sensor has favorable precision and reproducibility, and it also proved that the electrochemical sensor has outstanding stability for the detection of p-aminophenol [39]. In addition, other different electrochemical sensors for p-aminophenol were compared with the present work and the results are shown in Table 2. The results showed that the established method had high sensitivity and precision for the detection of p-aminophenol under the electric signal enhancement effect catalyzed by Fe_3O_4@Au/MOF mimic enzyme.

In this work, six common substances in food wastewater were selected as interfering substances to evaluate the anti-interference performance of the electrochemically enhanced p-aminophenol detection system. Tyrosine, cysteic acid, glucose, $CuCl_2$, NaCl, and K_2SO_4 with a concentration of 0.25 mol L^{-1} were selected as interfering substances, and p-aminophenol with a concentration of 2.5 mmol L^{-1} was used as a reference system for comparative study. The concentration of interfering substances was 100 times that of p-aminophenol. As shown in Fig. 9, compared with higher concentrations of interfering substances, the detection system showed a significant current response to p-aminophenol. It showed that the electrochemical enhancement system based on Fe_3O_4@Au/MOF mimic enzyme exhibited good selectivity and anti-interference performance for the detection of p-aminophenol.

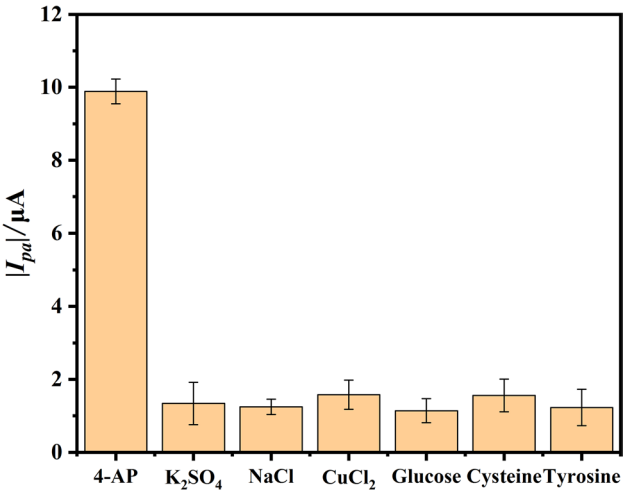

Fig. 9 Selectivity of the assay for p-aminophenol compared to other potential interferences. The concentration of p-aminophenol is 2.5 mmol L^{-1}, and other interferences concentration are 0.25 mol L^{-1}. Error bars represent the standard derivation (SD) of replicates measurements with $n = 3$

3.6 Real sample analysis

The method of adding different concentrations of p-aminophenol standard solutions to the tap water in the laboratory was selected to evaluate the practical sample practicability of the established electrochemical detection method. According to the optimized electrochemical-enhanced detection system, the oxidation peak current values of the three sample solutions of different concentrations were detected and brought into the regression equation of the working curve to determine the recovery rate of the standard addition and evaluate the accuracy of the detection system. The results are shown in Table 3. The electrochemical sensor to determine the concentration of p-aminophenol in laboratory tap water is in good agreement with the HPLC method [44]. Moreover the standard addition recovery rate of the enhanced detection system was 96.4–101.8% and the RSD is less than 3.59%, indicating that the electrochemical-enhanced detection system had a good addition recovery rate

Table 2 Comparison of different electrochemical sensors for p-aminophenol detection

Electrochemical sensors	Method	Linear range/ mmol L^{-1}	LOD/μmol L^{-1}	References
VMSF/ITO electrode	DPV	0.5–400	0.32	[44]
Poly(3,4-ethylenedioxythiophene)/GCE	DPV	4–320	1.20	[45]
$Au_{0.5}Pt_{0.5}$/ZnO	CV/CA		3.60	[46]
Fc-PAA-AuNPs/GCE	CV	30–1064	7.61	[47]
Microfluidic paper-based device		0.05–2000	10.00	[48]
G-PANI/CPE	CV	50–500	15.68	[49]
Fe_3O_4@Au/MOF peroxidase-like	CV	0.1–10	0.38	This work

Table 3 Analytical results of p-aminophenol in real samples

Samples	Added/g L^{-1}	HPLC/g L^{-1}	Found/g L^{-1}	Recovery rate/%	R.S.D/%
Laboratory tap water	0.5	0.494	0.482	96.4	2.81
	1	0.997	1.018	101.8	3.14
	2.5	2.502	2.468	98.7	3.58

and precision for samples. The detection of p-aminophenol in actual samples can be realized.

4 Conclusion

In summary, an electrochemical sensor based on Fe_3O_4@Au/MOF has been successfully constructed, which has enhanced peroxidase-like properties and realizes high-efficiency real-time monitoring of p-aminophenol. Fe_3O_4@Au/MOF synthesized via a simple self-assembly method could catalyze the oxidation–reduction reaction of p-aminophenol by H_2O_2. Based on it, p-aminophenol detection could be realized. The electrochemical sensor exhibited higher sensitivity and stronger anti-interference ability to coexisting molecules, as well as possessed a linear electrochemical response to p-aminophenol within a more comprehensive concentration range. The electrochemical sensor exhibited excellent sensing performance in aqueous samples. Therefore, Fe_3O_4@Au/MOF electrochemical sensor exhibited the potential to detect environmental pollutants.

Acknowledgements This work was supported by the National Natural Science Foundation of China (No. 31370649 and 31201376), the China Postdoctoral Science Foundation (No. 2014T70304 and 2013M531009), the Heilongjiang Postdoctoral Fund (No. LBH-Z13002), the Natural Science Foundation of Heilongjiang Province of China (No. C2016034), the Harbin University of Commerce Youth Innovation Talents (No. 2019CX05), the Heilongjiang Province Leading Talent Support Program (No. 2020376), the Graduate Research Innovation Project of Harbin University of Commerce (No. HSD20210705), and the Heilongjiang Postdoctoral Fund (No. LBH-Q19027).

Declarations

Conflict of interest The authors have no financial or proprietary interests in any material discussed in this article.

References

1. Jin Y, Yan B (2021) A bi-functionalized metal-organic framework based on N-methylation and Eu^{3+} post-synthetic modification for highly sensitive detection of 4-aminophenol (4-AP), a biomarker for aniline in urine. Talanta 227:122209. https://doi.org/10.1016/j.talanta.2021.122209
2. Shaban SM, Moon BS, Kim DH (2021) Selective and sensitive colorimetric detection of p-aminophenol in human urine and paracetamol drugs based on seed-mediated growth of silver nanoparticles. Environ Technol Innov 22:101517. https://doi.org/10.1016/j.eti.2021.101517
3. Shaban SM, Moon BS, Pyun DG, Kim DH (2021) A colorimetric alkaline phosphatase biosensor based on p-aminophenol-mediated growth of silver nanoparticles. Colloids Surf B 205:111835. https://doi.org/10.1016/j.colsurfb.2021.111835
4. DeSouza JC, Zanoni MVB, Oliveira-Brett AM (2020) Genotoxic permanent hair dye precursors p-aminophenol and p-toluenediamine electrochemical oxidation mechanisms and evaluation in biological fluids. J Electroanal Chem 857:113509. https://doi.org/10.1016/j.jelechem.2019.113509
5. Shi P, Xue R, Wei Y, Lei X, Ai J, Wang T, Yang W (2020) Gold nanoparticles/tetraaminophenyl porphyrin functionalized multiwalled carbon nanotubes nanocomposites modified glassy carbon electrode for the simultaneous determination of p-acetaminophen and p-aminophenol. Arab J Chem 13(1):1040–1051. https://doi.org/10.1016/j.arabjc.2017.09.008
6. Li M, Ding C, Jia P, Guo L, Wang S, Guo Z, Huang Y (2021) Semi-quantitative detection of p-Aminophenol in real samples with colorfully naked-eye assay. Sens Actuators B Chem 334:129604. https://doi.org/10.1016/j.snb.2021.129604
7. Zhao Q, Zheng X, Xing L, Tang Y, Zhou X, Hu L, Yan Z (2021) 2D Co_3O_4 stabilizing Rh nano composites developed for visual sensing bioactive urea and toxic p-aminophenol in practice by synergetic-reinforcing oxidase activity. J Hazard Mater 409:125019. https://doi.org/10.1016/j.jhazmat.2020.125019
8. Nemakal M, Aralekallu S, Mohammed I, Pari M, Sannegowda LK (2019) Nanomolar detection of 4-aminophenol using amperometric sensor based on a novel phthalocyanine. Electrochim Acta 318:342–353. https://doi.org/10.1016/j.electacta.2019.06.097
9. Boltia SA, Soudi AT, Elzanfaly ES, Zaazaa HE (2019) Development and validation of chromatographic methods for simultaneous determination of paracetamol, orphenadrine citrate and caffeine in presence of p-aminophenol; quantification of p-aminophenol nephrotoxic impurity using lc–ms/ms. J Chromatogr Sci 58(3):223–233. https://doi.org/10.1093/chromsci/bmz094
10. Goclik E, Chrzescijanska E, Kusmierek E, Rynkowski J (2019) Electroanalytical and spectrophotometric determination of n-acetyl-p-aminophenol in pharmaceuticals. Port Electrochim Acta 37(6):345–357. https://doi.org/10.4152/pea.201906345
11. Zarei AR, Sadeghi HB, Reza M, Moghadam K (2018) Application of mixed micelle-mediated extraction for selective separation and spectrophotometric determination of p-aminophenol impurity in pharmaceutical formulations. Anal Bioanal Chem Res 5(1):1–9. https://doi.org/10.22036/abcr.2017.87476.1146
12. Balbaied T, Hogan A, Moore E (2020) Electrochemical detection and capillary electrophoresis: comparative studies for alkaline phosphatase (alp) release from living cells. Biosensors 10(8):95. https://doi.org/10.3390/bios10080095
13. Zhang Y, Zhang Y, Zhu L, He P, Wang Q (2019) High sensitivity detection of escherichia coli based on the measurement of β-galactosidase activity by microchip capillary electrophoresis combined with field-amplified sample injection. Anal Methods 11(11):1558–1565. https://doi.org/10.1039/C9AY00067D
14. Lu X, Wei F, Xu G, Wu Y, Yang J, Hu Q (2017) Surface molecular imprinting on silica-coated CdTe quantum dots for selective and sensitive fluorescence detection of p-aminophenol

in water. J Fluoresc 27(1):181–189. https://doi.org/10.1007/s10895-016-1944-7
15. Smsab C, Bsm A, Dhka B (2021) Selective and sensitive colorimetric detection of p -aminophenol in human urine and paracetamol drugs based on seed-mediated growth of silver nanoparticles. Environ Technol Innov 22:101517. https://doi.org/10.1016/j.eti.2021.101517
16. Smsab C, Bsm A, Dgp D, Dhka B (2021) A colorimetric alkaline phosphatase biosensor based on p -aminophenol-mediated growth of silver nanoparticles. Colloids Surf B 205:111835. https://doi.org/10.1016/j.colsurfb.2021.111835
17. Singh M, Sahu A, Mahata S, Singh PK, Rai VK (2019) Efficient electrochemical determination of p-aminophenol using a novel tricomponent graphene-based nanocomposite. New J Chem 43(37):14972–14978. https://doi.org/10.1039/C9NJ03680F
18. Thiruppathi M, Lin PY, Chou YT, Ho HY, Wu LC, Ho JAA (2019) Simple aminophenol-based electrochemical probes for non-enzymatic, dual amperometric detection of NADH and hydrogen peroxide. Talanta 200:450–457. https://doi.org/10.1016/j.talanta.2019.03.083
19. Zhao H, Xing Z, Su S, Song S, Zhou W (2020) Recent advances in metal organic frame photocatalysts for environment and energy applications. Appl Mater Today 21:100821. https://doi.org/10.1016/j.apmt.2020.100821
20. Wang J, Bao M, Wei T, Wang Z, Dai Z (2019) Bimetallic metal-organic framework for enzyme immobilization by biomimetic mineralization: constructing a mimic enzyme and simultaneously immobilizing natural enzymes. Anal Chim Acta 1098:148–154. https://doi.org/10.1016/j.aca.2019.11.039
21. Lmka B, Vii A, Jp C, Kkb D (2019) Metal-organic frameworks as materials for applications in sensors. Mendeleev Commun 29(4):361–368. https://doi.org/10.1016/j.mencom.2019.07.001
22. Li T, Bai Y, Wang Y, Xu H, Jin H (2020) Advances in transition-metal (Zn, Mn, Cu)-based MOFs and their derivatives for anode of lithium-ion batteries. Coord Chem Rev 410:213221. https://doi.org/10.1016/j.ccr.2020.213221
23. Song Y, Cho D, Venkateswarlu S, Yoon M (2017) Systematic study on preparation of copper nanoparticle embedded porous carbon by carbonization of metal–organic framework for enzymatic glucose sensor. RSC Adv 7(17):10592–10600. https://doi.org/10.1039/C7RA00115K
24. Huang X, Xu C, Ma J, Chen F (2018) Ionothermal synthesis of Cu-doped Fe_3O_4 magnetic nanoparticles with enhanced peroxidase-like activity for organic wastewater treatment. Adv Powder Technol 29(3):796–803. https://doi.org/10.1016/j.apt.2017.12.025
25. Zhang Y, Villarreal E, Li GG, Wang W, Wang H (2020) Plasmonic nanozymes: engineered gold nanoparticles exhibit tunable plasmon-enhanced peroxidase-mimicking activity. J Phys Chem Lett 11(21):9321–9328. https://doi.org/10.1021/acs.jpclett.0c02640
26. Wu Y, Ma Y, Xu G, Wei F, Ma Y, Song Q, Hu Q (2017) Metal-organic framework coated Fe_3O_4 magnetic nanoparticles with peroxidase-like activity for colorimetric sensing of cholesterol. Sens Actuators B 249:195–202. https://doi.org/10.1016/j.snb.2017.03.145
27. Goyal A, Kapoor S, Samuel P, Singhal S (2016) Magnetically retrievable modified nickel ferrite nanoparticles: efficient catalytic reduction of nitroarenes and photo-oxidation of hazardous dyes. Anal Chem Lett 6(2):98–123. https://doi.org/10.1080/22297928.2016.1188724
28. Wang Y, Gao J, Liu Y, Li M, Zhang M, He G, Sun Z (2021) Facile fabrication of ZnO nanorods modified Fe_3O_4 nanoparticles with enhanced magnetic, photoelectrochemical and photocatalytic properties. Opt Mater 111:110608. https://doi.org/10.1016/j.optmat.2020.110608
29. Deshmukh AR, Aloui H, Kim BS (2021) Novel biogenic gold nanoparticles catalyzing multienzyme cascade reaction: glucose oxidase and peroxidase mimicking activity. Chem Eng J 421:127859. https://doi.org/10.1016/j.cej.2020.127859
30. Alim S, Vejayan J, Yusoff MM, Kafi AKM (2018) Recent uses of carbon nanotubes & gold nanoparticles in electrochemistry with application in biosensing: a review. Biosens Bioelectron 121:125–136. https://doi.org/10.1016/j.bios.2018.08.051
31. Guan H, Peng B, Gong D, Han B, Zhang N (2021) Electrochemical enhanced detection of uric acid based on peroxidase-like activity of Fe_3O_4@Au. Electroanalysis 33(7):1736–1745. https://doi.org/10.1002/elan.202100036
32. Guan H, Liu B, Gong D, Peng B, Han B, Zhang N (2021) Direct electrochemical enhanced detection of dopamine based on peroxidase-like activity of Fe_3O_4@Au composite nanoparticles. Microchem J 164:105943. https://doi.org/10.1016/j.microc.2021.105943
33. Guan H, Song Y, Han B, Gong D, Zhang N (2020) Colorimetric detection of cholesterol based on peroxidase mimetic activity of GoldMag nanocomposites. Spectrochim Acta Part A 241:118675. https://doi.org/10.1016/j.saa.2020.118675
34. Zhidkov IS, Kurmaev EZ, Cholakh SO, Fazio E, D'urso L (2020) XPS study of interactions between linear carbon chains and colloidal Au nanoparticles. Mendeleev Commun 30(3):285–287. https://doi.org/10.1016/j.mencom.2020.05.007
35. Meeran MN, Saravanan SP, Shkir M, Kannan SK (2021) Fabrication of transition-metal (Zn, Mn, Cu)-based MOFs as efficient sensor materials for detection of H_2 gas by clad modified fiber optic gas sensor technique. Opt Fiber Technol 65:102614. https://doi.org/10.1016/j.yofte.2021.102614
36. Chen S, Huang R, Zou J, Liao D, Yu J, Jiang X (2020) A sensitive sensor based on MOFs derived nanoporous carbons for electrochemical detection of 4-aminophenol. Ecotoxicol Environ Saf 191:110194. https://doi.org/10.1016/j.ecoenv.2020.110194
37. Niu X, Bo X, Guo L (2021) Ultrasensitive simultaneous voltammetric determination of 4-aminophenol and acetaminophen based on bimetallic MOF-derived nitrogen-doped carbon coated CoNi alloy. Anal Chim Acta 1145:37–45. https://doi.org/10.1016/j.aca.2020.12.020
38. Shaikshavali P, Reddy TM, Palakollu VN, Karpoormath R, Rao YS, Venkataprasad G, Gopal P (2019) Multi walled carbon nanotubes supported CuO-Au hybrid nanocomposite for the effective application towards the electrochemical determination of acetaminophen and 4-aminophenol. Synth Met 252:29–39. https://doi.org/10.1016/j.synthmet.2019.04.009
39. Zhang Y, Zhang W, Zhang L, Song G, Wang N, Xu W, Huang W (2021) A molecularly imprinted electrochemical BPA sensor based on multi-walled carbon nanotubes modified by CdTe quantum dots for the detection of Bisphenol A. Microchem J 170:106737. https://doi.org/10.1016/j.microc.2021.106737
40. Gao Y, Wu K, Li H, Chen W, Fu M, Yue K, Liu Q (2018) Glutathione detection based on peroxidase-like activity of Co_3O_4–montmorillonite nanocomposites. Sens Actuators B 273:1635–1639. https://doi.org/10.1016/j.snb.2018.07.091
41. Su L, Qin W, Zhang H, Rahman ZU, Ren C, Ma S, Chen X (2015) The peroxidase/catalase-like activities of MFe_2O_4 (M= Mg, Ni, Cu) MNPs and their application in colorimetric biosensing of glucose. Biosens Bioelectron 63:384–391. https://doi.org/10.1016/j.bios.2014.07.048
42. Zhang Y, Zhou Z, Wen F, Tan J, Peng T, Luo B, Yin S (2018) A flower-like MoS_2-decorated $MgFe_2O_4$ nanocomposite: Mimicking peroxidase and colorimetric detection of H_2O_2 and glucose. Sens Actuators B 275:155–162. https://doi.org/10.1016/j.snb.2018.08.051
43. Alizadeh N, Salimi A, Sham TK, Bazylewski P, Fanchini G, Fathi F, Soleimani F (2021) Hierarchical $Co(OH)_2$/FeOOH/WO_3 ternary nanoflowers as a dual-function enzyme with pH-switchable

peroxidase and catalase mimic activities for cancer cell detection and enhanced photodynamic therapy. Chem Eng J 417:129134. https://doi.org/10.1016/j.cej.2021.129134
44. Liu X, Li H, Zhou H, Liu J, Li L, Liu J, Luo T (2020) Direct electrochemical detection of 4-aminophenol in pharmaceuticals using ITO electrodes modified with vertically-ordered mesoporous silica-nanochannel films. J Electroanal Chem 878:114568. https://doi.org/10.1016/j.jelechem.2020.114568
45. Mehretie S, Admassie S, Hunde T, Tessema M, Solomon T (2011) Simultaneous determination of N-acetyl-p-aminophenol and p-aminophenol with poly (3, 4-ethylenedioxythiophene) modified glassy carbon electrode. Talanta 85(3):1376–1382. https://doi.org/10.1016/j.talanta.2011.06.019
46. Fiaschi G, Cosentino S, Pandey R, Mirabella S, Strano V, Maiolo L, Shacham-Diamand Y (2018) A novel gas-phase mono and bimetallic clusters decorated Zno nanorods electrochemical sensor for 4-aminophenol detection. J Electroanal Chem 811:89–95. https://doi.org/10.1016/j.jelechem.2018.01.027
47. Elancheziyan M, Senthilkumar S (2021) Redox-active gold nanoparticle-encapsulated poly (amidoamine) dendrimer for electrochemical sensing of 4-aminophenol. J Mol Liq 325:115131
48. Shiroma LY, Santhiago M, Gobbi AL, Kubota LT (2012) Separation and electrochemical detection of paracetamol and 4-aminophenol in a paper-based microfluidic device. Anal Chim Acta 725:44–50. https://doi.org/10.1016/j.aca.2012.03.011
49. Rattanarat P, Suea-Ngam A, Ruecha N, Siangproh W, Henry CS, Srisa-Art M, Chailapakul O (2016) Graphene-polyaniline modified electrochemical droplet-based microfluidic sensor for high-throughput determination of 4-aminophenol. Anal Chim Acta 925:51–60. https://doi.org/10.1016/j.aca.2016.03.010